Target detection of hyperspectral images based on their Fourier spectral features

Khairul-Muzzammil Saipullah
Deok-Hwan Kim

Target detection of hyperspectral images based on their Fourier spectral features

Khairul-Muzzammil Saipullah
Universiti Teknikal Malaysia Melaka
Faculty of Electronic and Computer Engineering
(06) 5552160, Malaysia

Deok-Hwan Kim
Inha University
Department of Electronic Engineering
032 860 7424, Republic of Korea
E-mail: deokhwan@inha.ac.kr

Abstract. Original spectral features contain information pertinent to certain target spectral features. Without an efficient spectral feature extraction method, the target detection performance might be degraded. We present spectral feature extraction techniques based on the Fourier domain for use in target detection. These feature extraction methods are the Fourier magnitude (FM), Fourier phase (FP), and Fourier coefficient selection (FCS) methods. In our target detection experiments, we compared the proposed methods to the principle component analysis (PCA) and independent component analysis (ICA) methods and the original spectral features. The experiment results show that the FCS target detection accuracy is 95.75%, whereas the accuracies of the FM, FP, PCA, ICA methods, and the original spectral features are 86.76%, 36.28%, 84.51%, 74.49%, and 78.92%, respectively. The average feature extraction times of the proposed methods are 223% faster than that found for the PCA and 304% faster than the ICA methods. © *2012 Society of Photo-Optical Instrumentation Engineers (SPIE).* [DOI: 10.1117/1.OE.51.11.111704]

1 Introduction

With the development of the hyperspectral sensor, researchers in the remote sensing field are now able to extract ample spectral information to identify and discriminate between the spectral similarities of materials. The hyperspectral image (HSI) covers a large number of bands, which results in more accurate and detailed information regarding each material compared with other remotely sensed data, such as multispectral images. A typical HSI covers up to several hundred bands. Although a HSI provides more information, it has some disadvantages. Due to a huge number of dimensions in a HSI, an extremely high computational complexity is required. The greater the number of dimensions, the worse the discrimination becomes[1]; this is because a HSI contains a huge amount of spectral redundancy.[2] Therefore, the reduction of the spectral dimensionality is indispensable in performing classification or target detection.

The most widely used algorithm for dimensionality reduction in the remote sensing field is the principal component analysis (PCA).[3] The PCA computes orthogonal projections that maximize the amount of data variance, and yields a dataset in a new uncorrelated coordinate system. An improvement to the PCA is the independent component analysis (ICA),[4] which uses higher order statistics. Some other methods utilize multiscale approaches, such as derivative spectroscopy[5] and the wavelet transform,[6] to extract relevant features from hyperspectral signals. In the derivative spectroscopy method, a smoothing operator and a derivative operator are used to detect "hills" and "valleys" in the spectral curves, whereas in the wavelet transform method, the means of hyperspectral curves using windows of various widths are applied during the feature extraction.

In single target spectral detection, one needs to discriminate between the target class and the background, which usually contains more than 10 material classes. Although all of the dimensionality reduction methods are able to reduce the number of spectral bands and extract informative data regarding the spectral features, the effectiveness of the target detection feature recognition through the PCA or ICA methods is usually low and consumes a large amount of processing time. Therefore, the thrust of this research was to develop a fast and effective feature extraction method of the spectral features used for target detection.

In this paper, we present three target detection spectral feature extraction techniques based in the Fourier domain. These feature extraction methods are: Fourier magnitude (FM), Fourier phase (FP), and Fourier coefficient selection (FCS). For the FM and FP methods, the spectral features were converted into the Fourier domain and the magnitude and the phase of the Fourier complex coefficient were selected as the spectral feature. In regards to the FCS method, the real and the imaginary coefficients of the spectra's Fourier complex coefficient were compared. The real coefficients that were larger than the imaginary coefficients and the imaginary coefficients that were smaller than the real coefficients were selected for the spectral feature. This FCS technique employed the significant information extracted from the real and imaginary coefficients as being successfully applied in the feature extraction of the texture images.[7,8] Because the Fourier domain groups the coefficients from the most significant data to the least significant data, we easily selected the most significant data to reduce the dimensionality of the spectral feature. Moreover, through the use of the fast Fourier transform method, the computation of the FCS, FM, and FP consumed only a small amount of time.

The feature extraction methods were evaluated through the detection of three real targets placed on the ground before

the HSI was taken. Three target detection algorithms, the matched filter (MF), generalized likelihood ratio test (GLRT), and adaptive coherence/cosine estimator (ACE) methods were tested along with the spectral feature extraction methods. The remainder of this paper is organized as follows: Sec. 2 presents related work, Sec. 3 presents the detailed algorithms of the proposed feature extraction methods based on the Fourier domain phase, the experiment evaluations are described in Sec. 4, and the conclusions and future work are discussed in Sec. 5.

2 Related Works

2.1 *Principle Component Analysis*

Milton et al.[3] used the PCA to reduce the spectra dimensionality. The spectra can be converted to the relevant dimensionality by a linear transformation with the significant eigenvectors computed from the PCA. When the eigenvectors are convolved with the spectra, they transform the spectra into fewer data points. The eigenvectors are determined by computing the covariance matrix of the mean of the spectral data matrix by:

$$[C_{jk}] = \frac{\sum_{i=1}^{n} X_{ij} X_{ik} - \frac{\sum_{i=1}^{n} X_{ij} \sum_{i=1}^{n} X_{ik}}{N}}{N-1}, \tag{1}$$

where $[C_{jk}]$ is the covariance matrix of the mean, X is a single band measurement, N is the number of spectra in the matrix, j and k are indices over the spectral bands, and i is an index over the number of spectra. The covariance matrix is then diagonalized by finding a matrix Q in such a manner that:

$$[Q]^{-1}[C][Q] = [\lambda][I], \tag{2}$$

where I is the identity matrix. The columns of matrix Q are the eigenvectors and the column matrix λ represents the corresponding eigenvalues. Matrix λ is then sorted in descending order. The resulting PCA feature is the element of matrix Q corresponding to the sorted eigenvalues indices. The sorted matrix Q is also named as the principle component of the spectra data. The principle component is sorted from the significant eigenvectors to the less significant eigenvectors. These eigenvectors are then used as the feature vectors of the spectra.

2.2 *The ICA*

The goal of the principle component analysis is to minimize the reprojection error found in compressed data. The goal of the ICA is to minimize the statistical dependence between the basis vectors. Mathematically, this calculation can be written as:

$$\mathbf{WX^T} = \mathbf{U}, \tag{3}$$

where the ICA finds the linear transformation W that minimizes the statistical dependence between the rows of U given by data matrix X. The basis vectors in the ICA are neither orthogonal nor ranked in order. There are a great many algorithms used to find W The algorithm proposed by Kolenda et al.[9] will be applied. This ICA algorithm is an enhanced

version of the Molgedey and Schuster algorithm[4] that possesses a fast computation of the model. Let $\mathbf{X}_\tau = \{\mathbf{X}_{j,t+\tau}\}$ be the time shifted data matrix where $\mathbf{X}_{j,t}$ is the frequency of the j'th term during time t. The lag parameter τ is automatically determined by exploiting the difference between the autocorrelations of the data matrix $\mathbf{X}$. Then by using the singular value decomposition (SVD) method, the principle component subspace is calculated by decomposing:

$$\mathbf{X} = \mathbf{UDV^T}. \tag{4}$$

The quotient matrix can now be written as:

$$\hat{\mathbf{Q}} = \frac{1}{2}\mathbf{D}(\mathbf{V}_\tau^T \mathbf{V} + \mathbf{V}^T \mathbf{V}_\tau)\mathbf{D}^{-1} = \mathbf{\Phi}\mathbf{\Lambda}\mathbf{\Phi}^{-1}. \tag{5}$$

The $\mathbf{\Phi}$ contains the rectangular ICA basis projection onto the PCA subspace and $\mathbf{U}$ holds the projection from the PCA subspace. The estimated mixing matrix and the source signals are given by:

$$\mathbf{A} = \mathbf{U}\mathbf{\Phi} \tag{6}$$

$$\mathbf{S} = \mathbf{\Phi}^{-1}\mathbf{DV^T}. \tag{7}$$

$\mathbf{\Phi}$ can be selected according to the significant principle components. By only selecting a certain number of significant principle components after the SVD, the dimensions of the input data can be reduced. The final estimated source signals $\mathbf{S}$ are used as the feature vectors of the input data.

3 Proposed Method

This section presents the proposed feature extraction methods based on the Fourier domain, the FCS, FM, and FP methods. The first step was to transform the original spectral $s(n)$, $n = 0, 2, 3, \ldots, N+1$ into the Fourier domain. The Fourier transform and inverse transform of $s(n)$ are given by:

$$S(k) = \sum_{n=0}^{N-1} s(n) e^{-\frac{2\pi i}{N}kn} \tag{8}$$

$$s(n) = \frac{1}{N} \sum_{k=0}^{N-1} S(k) e^{-\frac{2\pi i}{N}kn}, \tag{9}$$

where N is the number of dimensions of spectral $s(n)$. Using Eq. (8), the original spectral $s(n)$ was converted to the Fourier coefficients $S(k)$. For the FM feature extraction technique, the magnitude of $S(k)$ was calculated using the following formula:

$$\mathrm{FM}(x) = \sqrt{\mathrm{Re}\{S(x)\}^2 + \mathrm{Im}\{S(x)\}^2}. \tag{10}$$

For the FP feature technique, the phase of $S(k)$ was calculated using the following formula:

$$\mathrm{FP}(x) = \tan^{-1}\left(\frac{\mathrm{Im}\{S(x)\}}{\mathrm{Re}\{S(x)\}}\right). \tag{11}$$
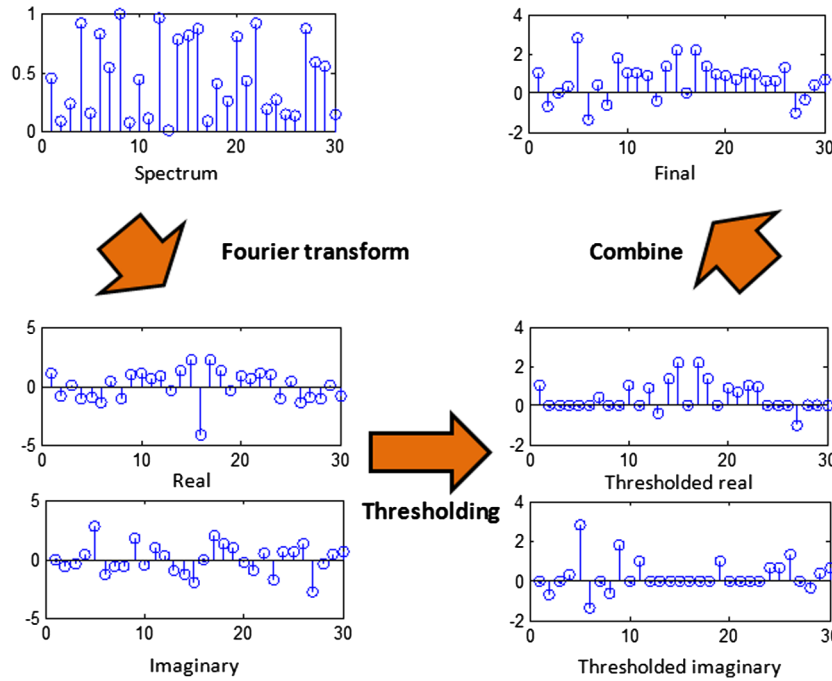
Fig. 1 The graphical explanation of the FCS method.

And finally, for the FCS feature technique, a combination of the selected real and imaginary coefficients of $S(k)$ was applied. The FCS was calculated using the following formula:

$$\text{FCS}(x) = R(x) + I(x), \tag{12}$$

where

$$R(x) = \begin{cases} \text{Re}\{S(x)\}, & \text{if } \text{Re}\{S(x)\} \geq \text{Im}\{S(x)\} \\ 0, & \text{otherwise} \end{cases}$$

$$I(x) = \begin{cases} \text{Im}\{S(x)\}, & \text{if } \text{Im}\{S(x)\} \geq \text{Re}\{S(x)\} \\ 0, & \text{otherwise} \end{cases}. \tag{13}$$

A graphical explanation of the FCS method is shown in Fig. 1. First, the Fourier transform of the spectrum is calculated. The first coefficient of the Fourier transform is very large compared with the other coefficients. For a clear graphical view of the Fourier coefficients, the first coefficient is normalized by dividing it by the sum of all of the coefficients. Note that the normalization does not affect the discrimination power of the feature extraction method. Because of this, the normalization is only done for the vivid graphical view of the coefficient and is not applied in the FCS to reduce the computation time. The Fourier transform will result in real and imaginary coefficients. Using Eq. (13), these coefficients are thresholded according to the conditions given in the formula. Finally, the thresholded real coefficient and the thresholded imaginary coefficient are combined as in Eq. (12).

In Eqs. (11)–(13), x is the desired dimension of the spectral feature, which is in the range of $0 \leq x < N/2$. The range of x is limited to one-half of the original spectral N dimension due to the redundancy of the Fourier transform of real numbers.[10] The Fourier coefficients $S(k)$ of a real number repeat themselves in $S(N/2)$. So only the halves of the Fourier coefficients $S(k)$ are significant. Because the Fourier domain groups the coefficients from the most significant data to the least significant data, the spectral feature can be easily reduced by selecting only the upper part $FM(x)$, $FP(x)$, and $FCS(x)$ within the range of $0 \leq x < N/2$.

The magnitude and the phase of the Fourier coefficients are the basic feature extraction techniques widely used in the image and audio processing fields.[11–13] Some studies were performed on texture discrimination that apply the FCS approach.[7,8] In these studies, the real Fourier coefficients were thresholded against the imaginary Fourier coefficients and converted into a binary code word. The approach used by the FCS was different from those studies in that the FCS does not only utilize the sign of the coefficients, but also
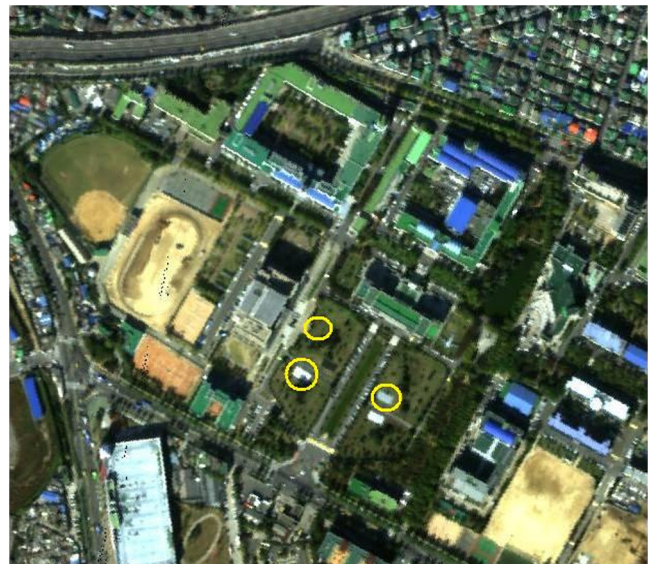

Fig. 2 The RGB bands of the Inha University hyperspectral image.

utilizes the value of the complex coefficients themselves. This produces a unique and specific pattern in regards to the FCS spectral feature, which is able to discriminate the spectral features used for target detection.

4 Experiment

This section discusses the experiment performed regarding the performance of the dimensionality reduction methods.

The methods are evaluated in terms of their spectral classification accuracy and their HSI segmentation accuracy.

4.1 Experimental Setup

In the experiment, the proposed methods, namely the FCS, FM, and FP, were evaluated in terms of detection accuracy using various feature dimensions, receiving operating characteristic curves, detection versus threshold curves, and time
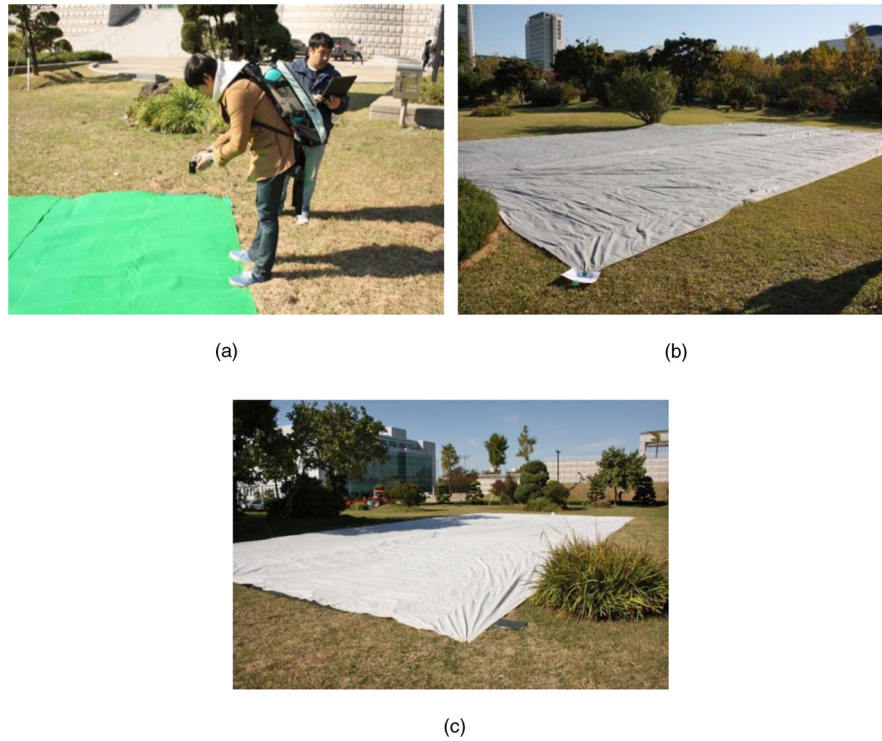

(a)   (b)

(c)

Fig. 3 The targets used in the experiment: (a) green nonwoven fabric, (b) gray canvas tarps, and (c) white canvas tarps.
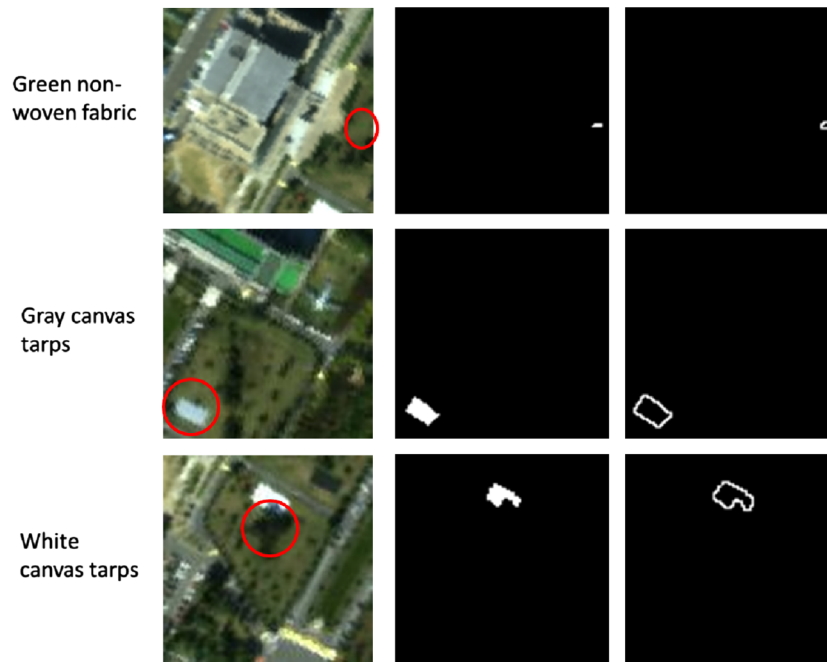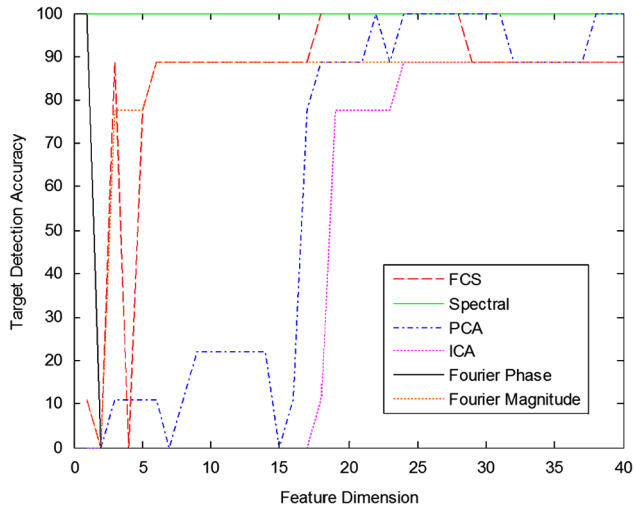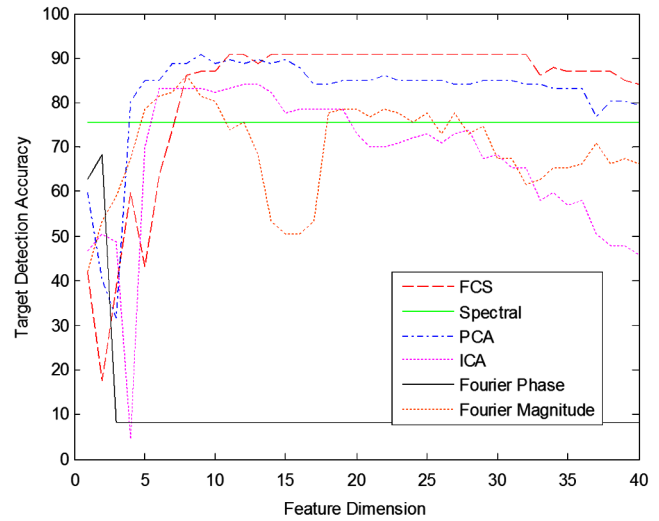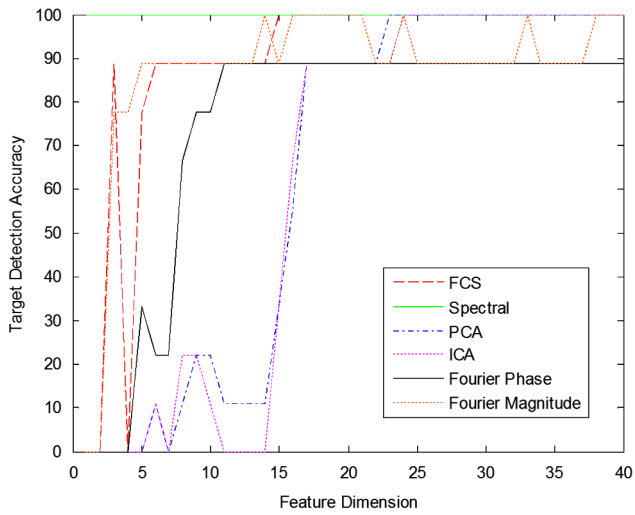

Fig. 4 The targets and their ground truth images, each row indicates the three different targets, the left column shows the targets, the center column shows the ground truth images of the targets, and the right column shows the boundary of the ground truth image.
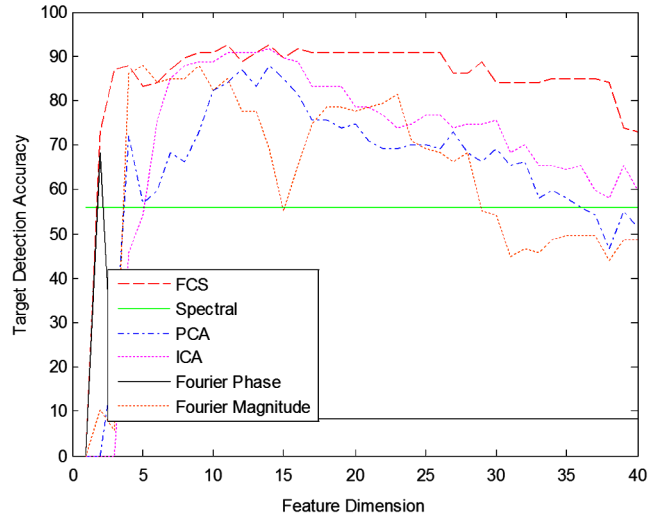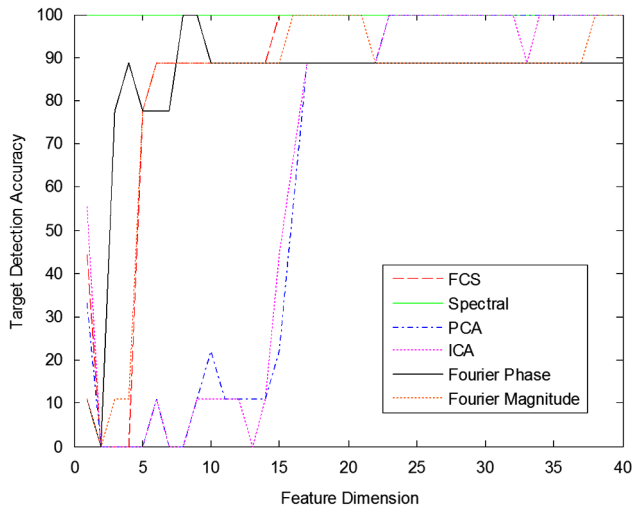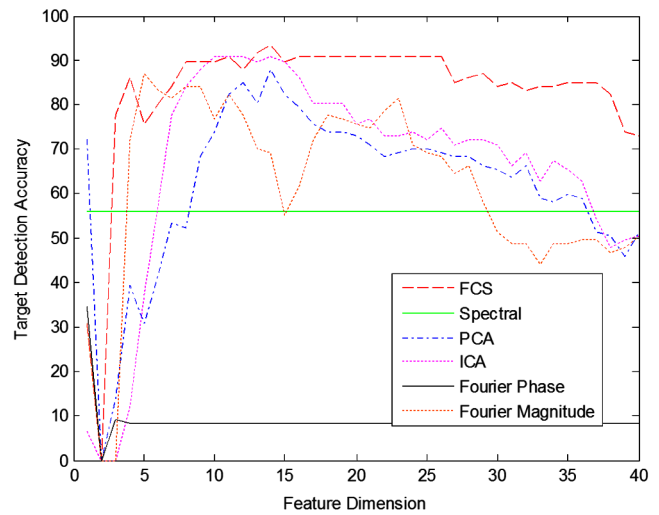
(a)

(b)

(c)

Fig. 5 The green nonwoven fabric detection accuracy according to method: (a) MF, (b) GLRT, and (c) ACE.

Fig. 6 The gray canvas tarp detection accuracy according to method: (a) MF, (b) GLRT, and (c) ACE.

efficiency. All of the experiments were executed on a computer with an Intel Core™ 2 Duo 2.33 GHz and 2 GB of main memory. The program was coded using MATLAB R2007a and the Windows XP operating system. The proposed FCS, FM, and FP methods were compared to original spectral features and two other dimensionality reduction features, the PCA and ICA methods discussed in Sec. 2.

A HSI of Inha University was used in the experiments. The resolution of the HSI is 545×618 pixels at a scale of 30 m per pixel. These HSIs were captured using Hyperion sensors with a total of 96 bands after removing the noise bands and the corrupted bands. The wavelengths of the bands range from 365.2 to 1044.6 nm. The Inha University HSI in the RGB bands is shown in Fig. 2. The three real targets that were implemented in the experiment are indicated by circles. The targets were a green nonwoven fabric, gray canvas tarps, and white canvas tarps placed on the Inha University lawn. The images of the targets are shown in Fig. 3. The ground truth images of the three targets were carefully created by observing the spectral features manually. The three targets, their ground truth images, and the boundary of the ground truth images are shown in Fig. 4.

The feature extraction methods were evaluated through the detection of three real targets that were placed on the ground before the HSI was taken. Three target detection algorithms, the MF,[14] GLRT,[15,16] and ACE[17,18] were performed using the spectral feature extraction methods. To evaluate the FCS, FM, and FP algorithms, the spectral feature extraction methods were compared to the PCA, ICA, and the original spectral features.

4.2 Experimental Results

The proposed FCS, FM, and FP methods were evaluated and compared with ICA, PCA, and the spectral feature methods through various experiments. The number of dimensions differs for the FCS, FM, FP, ICA, and PCA methods according to their setup, whereas the number of dimensions for the original spectral features always covers the entire 96 dimensional band. The first experiment measured the target detection accuracy using the various feature dimensions. Based on the results of the target detection accuracy experiment using the various feature dimensions, the most appropriate dimension number was selected for the target detection accuracy with fixed feature dimensions. Finally, the efficiency of the spectral feature extraction was assessed by computing the target detection time consumption for each feature extraction method and target detector. The target detection accuracy was measured using the following formula:

Detection accuracy

$$= \frac{\text{Number of correctly detected pixels of the target}}{\text{Total number of pixels of the target}}.$$

(14)

4.2.1 Target detection evaluation

To ensure that the three target detectors, namely the MF, GLRT, and ACE methods, could operate automatically, the detection threshold of those target detectors were determined. The detection threshold can be determined by using a constant false-alarm rate (CFAR) processor.[19] A CFAR provides detection thresholds that are relatively immune to noise
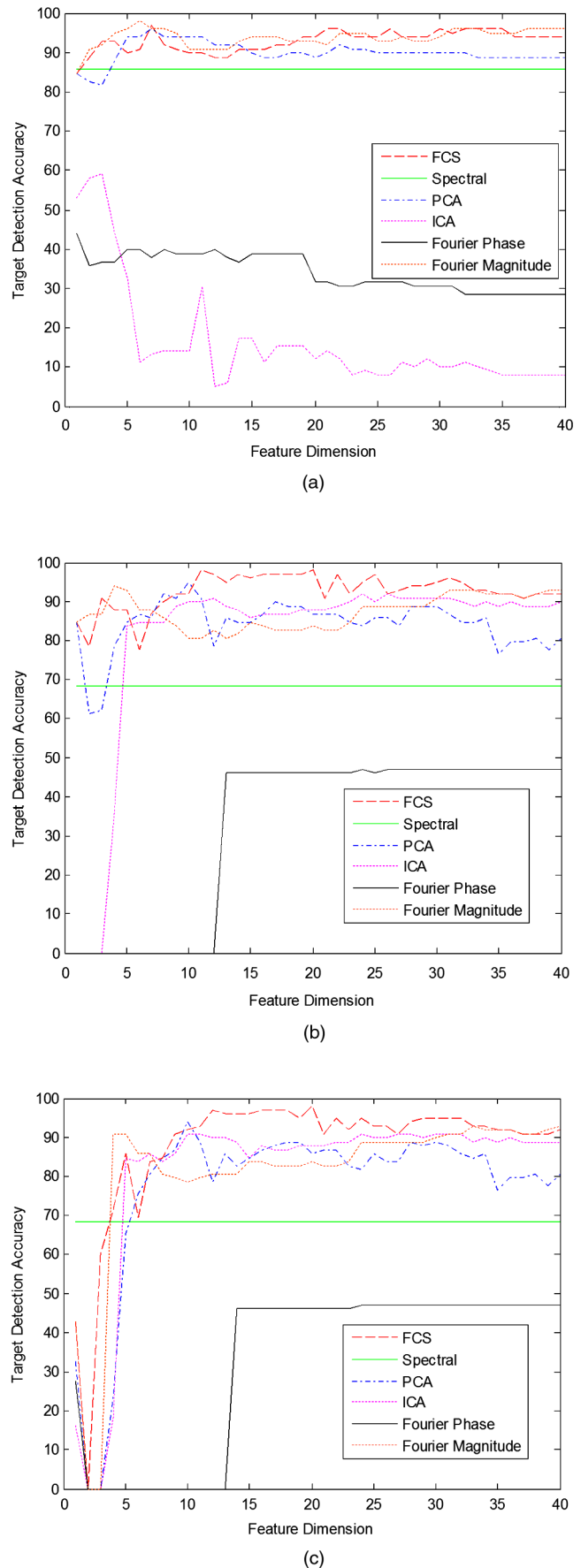

(a)

(b)

(c)

Fig. 7 The white canvas tarp detection accuracy according to method: (a) MF, (b) GLRT, and (c) ACE.
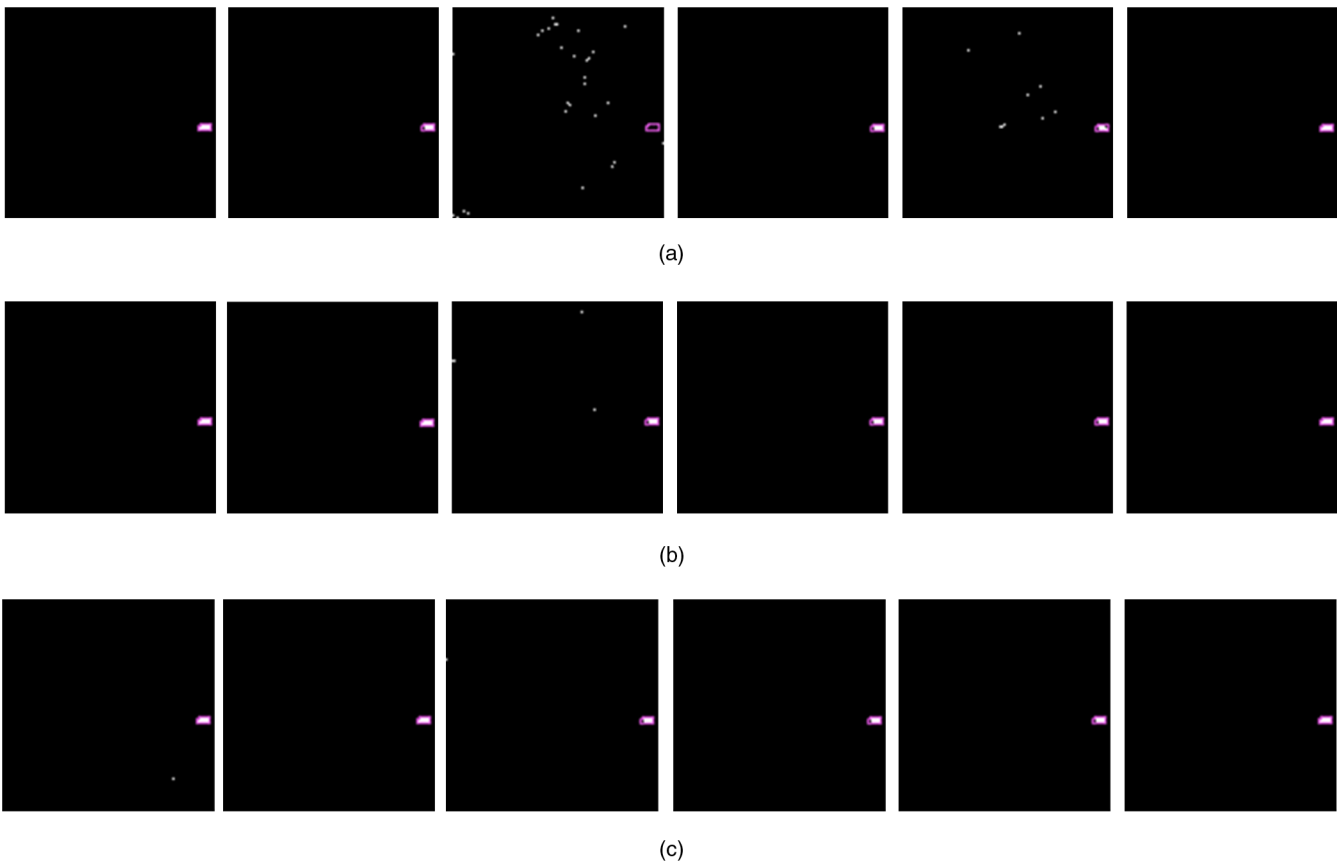
(a)

(b)

(c)

Fig. 8 The visual result of the green nonwoven fabric detection: (a) MF, (b) GLRT, and (c) ACE. White dots inside the target boundary are the true positives whereas outside the target boundary are the false positives; black is the background.

and background variations. By using an appropriate CFAR setting, target detection possessing a consistent false-alarm rate and high detection accuracy can be achieved. The performance of the original spectral feature can also be measured by scrutinizing how easily a threshold can be determined in maintaining a perfect balance between a low false alarm rate and high true positive or high correct target detection rate.[20] For this experiment, the CFAR was set to 0.001.

The target detection routines using the MF, GLRT, and ACE methods were repeated 40 times using different feature dimension sizes in the range from 1 to 40 dimensions. The target detection accuracies of the green nonwoven fabric using the MF, GLRT, and ACE methods with difference spectral features are shown in Fig. 5; the gray and white tarp results are shown in Figs. 6 and 7, respectively. As shown in Fig. 5, the target detection accuracy was unstable at the beginning ranging wildly until it stabilized at a range of 15 dimensions and above. Most of the feature dimension results show an increase to 90% target detection accuracy. For the spectral feature extraction, the range was 100% because the spectra were not used in feature extraction. Figure 6 shows the results for the gray canvas detection accuracy for different dimensions. In average, all the feature extraction increase in the 5 range and decrease when the range is 20 and above. From the graphs we can see that the FCS method was more stable than the other feature dimension methods. Figure 7 shows that the MF detector was better compared with the GLRT and ACE detectors,

the data was more stable and the difference percent of range was low.

From these results, it can be seen that by dimension = 20, the detection accuracy became stable and high for all of the features in the MF, GLRT, and ACE methods for all three targets. Therefore the feature dimension of 20 was selected to execute the later experiments. To see the accuracy of the target detection accuracy visually, the segmentation between the target and the background was performed on all of the targets using the MF, GLRT, and ACE target detectors using the proposed and the other feature extraction methods. All of the target detection was done using dimension
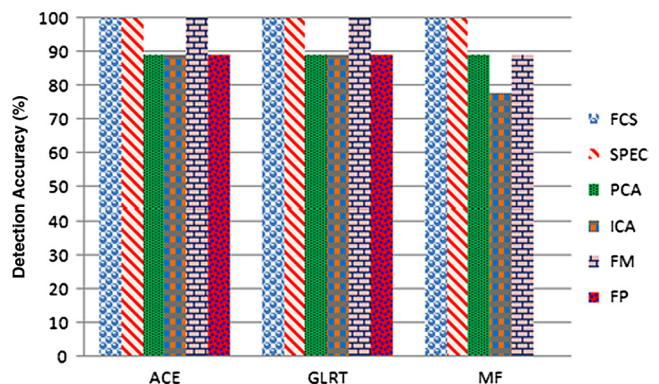

Fig. 9 The detection accuracy of green nonwoven fabric detection using MF, GLRT, and ACE target detectors.
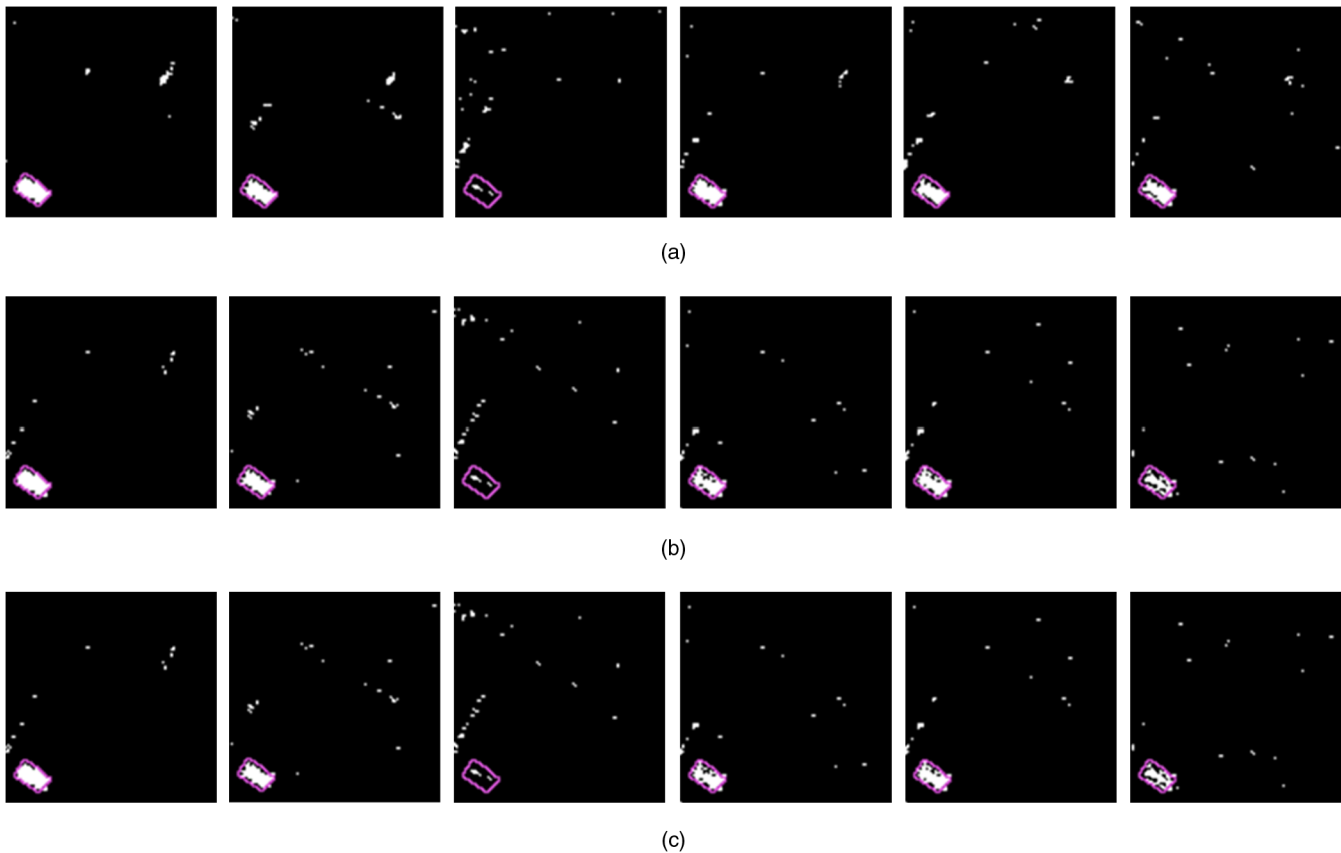
Fig. 10 The visual results of the gray canvas tarp detection: (a) MF, (b) GLRT, and (c) ACE. White dots inside the target boundary are the true positives whereas outside the target boundary are the false positives; black is the background.

$D = 20$, CFAR $= 0.001$. Figure 8 shows the target detection of the green nonwoven fabric. The target detection of this target was simple because the target was small and had a discriminative spectral feature. Most of the feature extraction methods were able to detect the whole target with a high true positive rate. Therefore, for the performance evaluation the detection of the false positives for each feature extraction method must also be observed.

Looking at Fig. 8, it can be clearly seen that the FP and the original spectral methods performed badly for the MF target detector, generating a high false positive rate compared with the other feature extraction methods. For the GLRT and ACE target detectors, all of the feature extraction methods performed well, with a high correlation for true positives and few false positives. This demonstrates the superior performance of the GLRT and ACE target detectors compared with the MF detector. For an accurate observation of the target detection accuracy, we refer to the bar plot shown in Fig. 9. For the MF detector bars, the FP feature extraction method was unable to detect any target. Compared with the MF, we can see from the bars that the ACE and GLRT target detectors are able to detect the target using all of the feature extraction methods. This shows the robustness of the ACE and GLRT detectors that can handle any type of input including the angle or phase. However, we were unable to conclude which detector or feature extraction method was better because the target was small and easy to detect. For a better comparison of the detectors and feature extraction methods, we analyzed the target detection

performance using the more difficult white and grey targets, because they were larger and contained more subpixels compared with the green nonwoven fabric.

Figure 10 shows the target detection of the gray canvas tarps. Most of the feature extractors were able to detect the entire target but were unable to get a 100% accurate high true positive rate. There were some false positives detected by the detectors with a higher rate compared with the green nonwoven fabric detection. This is because of the large number of subpixels in the target. Most of the subpixels were located near to boundary of the target. These subpixels are hard to classify because they contain
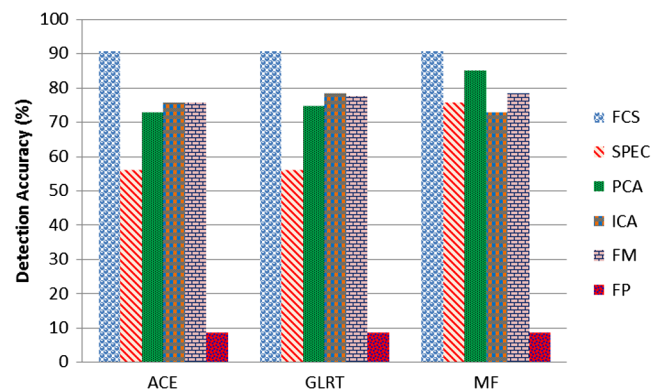

Fig. 11 The detection accuracy of gray canvas tarps detection using MF, GLRT, and ACE target detectors.

(a) FCS, FM, FP, PCA, ICA, SPECTRAL using MF

(b) FCS, FM, FP, PCA, ICA, SPECTRAL using GLRT

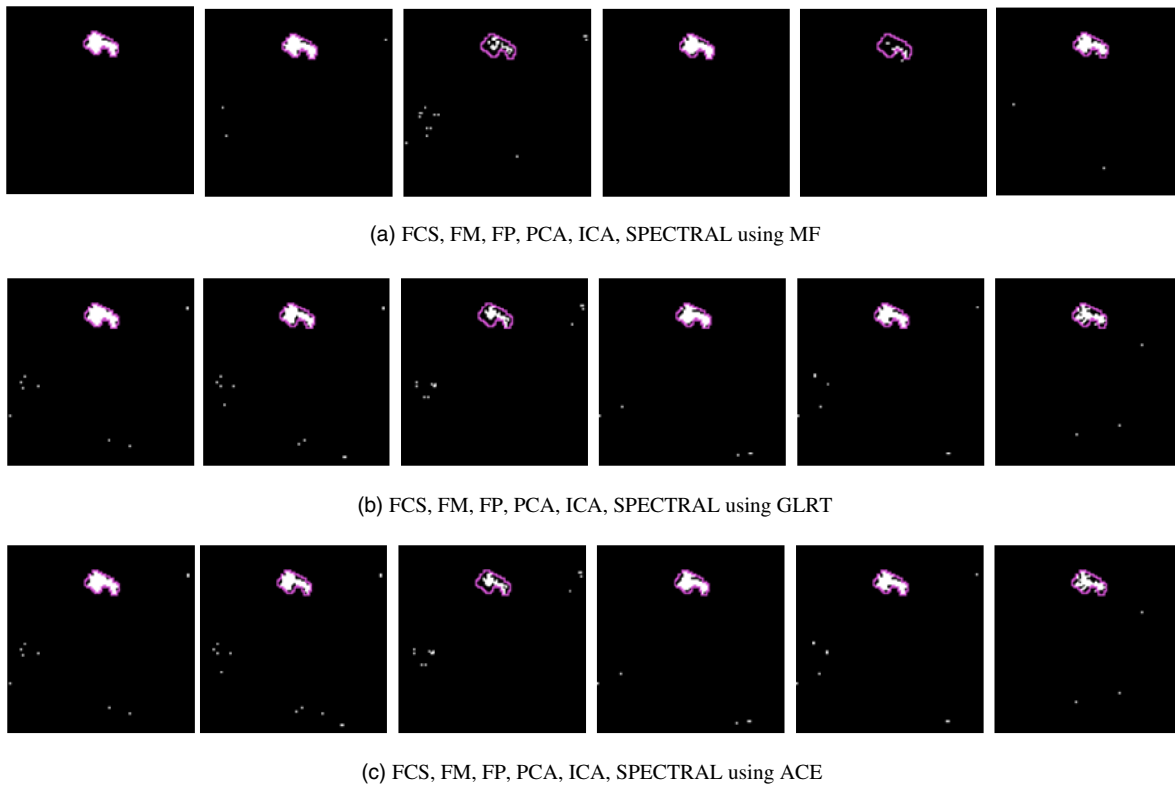(c) FCS, FM, FP, PCA, ICA, SPECTRAL using ACE

Fig. 12 The visual results of the white canvas tarp detection: (a) MF, (b) GLRT, and (c) ACE. White dots inside the target boundary are the true positives whereas outside the target boundary are the false positives; black is the background.

other material spectral information. We can see that the FP and SPEC performed badly in all of the target detectors compared with other feature extraction methods. For the case of SPEC, no feature extraction was done to the spectral, so it still contains the redundant and insignificant information in it. FP is based on the phase of the spectra that contains positive and negative signs of the angles. These angle values are extremely sensitive to translation or position even a small change to the vector of the element in spectral could change the sign or the phase value significantly. Because of this disadvantage, the performance of FP becomes inconsistent. For a better observation, we can see the bar plot of the accuracies as shown in Fig. 11. If we focus on the SPEC and PCA detection accuracies, the accuracies in ACE and GLRT are smaller than that of MF. This shows that MF could detect better using the raw spectra and eigenvectors compared with ACE and GLRT. But when it comes to Fourier transform based feature, ACE and GLRT perform better.

Figure 12 shows the target detection of the white canvas tarps. Most of the feature extraction methods were able to detect the entire target with a high true positive rate. From Fig. 12, the FP and ICA methods performed badly when the MF detector was employed. As explained before, MF is only good with the raw data and significant spectra vector (eigenvector) as implemented in PCA. Other approaches, such as ICA, perform badly in the MF. It can be seen that the FCS detector shows consistent accuracies in each target detector. To demonstrate the accurate observation of the target, we refer to the bar plot in Fig. 13. The performance between the GLRT and ACE detectors were similar with a small difference in accuracies ranging from

0.01% to 10% for each feature extraction method. The accuracy of FCS is slightly smaller in the MF compared with ACE and FCS. FCS is not based on the vector of the spectra so it performance might be lower in the MF.

4.2.2 The time consumption evaluation

Tables 1–3 show the time consumption in second (s) of the feature extractions (FE) and the target detections (DET) of the three targets using MF, ACE, and GLRT detectors. Each FE and DET operation underwent 100 iterations and the average time was recorded. The spectral method does not require feature extraction; its FE time is zero. From all of the tables, the target detection for Fourier
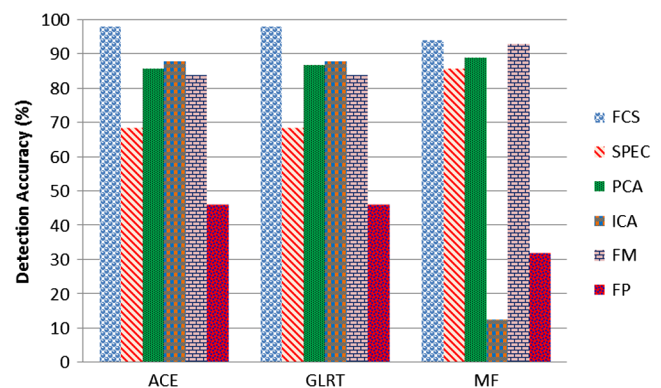

Fig. 13 The detection accuracy of white canvas tarps detection using MF, GLRT, and ACE target detectors.

Table 1 The time consumption in second of the feature extraction (FE) and target detection (DET) of the green nonwoven fabric.

Method	FE	ACE		GLRT		MF	
		DET	FE + DET	DET	FE + DET	DET	FE + DET
FCS	0.0765	0.1179	0.1944	0.1461	0.2226	0.0311	0.1075
FM	0.0554	0.1248	0.1802	0.1521	0.2075	0.0340	0.0894
FP	0.1002	0.2454	0.3456	0.2448	0.3449	0.3111	0.4113
PCA	17.8902	0.1435	18.0337	0.1860	18.0762	0.0217	17.9119
ICA	24.2299	0.3123	24.5422	0.3642	24.5941	0.0709	24.3008
SPEC	0.0000	0.1524	0.1524	0.2032	0.2032	0.0449	0.0449
TOTAL		1.0964	43.4486	1.2965	43.6487	0.5136	42.8658

Table 2 The time consumption in second of the feature extraction (FE) and target detection (DET) of the gray canvas tarps.

Method	FE	ACE		GLRT		MF	
		DET	FE + DET	DET	FE + DET	DET	FE + DET
FCS	0.0775	0.0722	0.1497	0.0934	0.1708	0.0730	0.1504
FM	0.0566	0.0653	0.1219	0.0844	0.1411	0.0808	0.1374
FP	0.0987	0.1029	0.2016	0.1201	0.2187	0.0453	0.1440
PCA	17.9362	0.0584	17.9945	0.0756	18.0117	0.0501	17.9863
ICA	24.4663	0.0581	24.5245	0.0668	24.5331	0.0744	24.5408
SPEC	0.0000	0.0706	0.0706	0.0941	0.0941	0.0969	0.0969
TOTAL		0.4276	43.0628	0.5343	43.1696	0.4206	43.0558

Table 3 The time consumption in second of the feature extraction (fe) and target detection (DET) of the white canvas tarps.

Method	FE	ACE		GLRT		MF	
		DET	FE + DET	DET	FE + DET	DET	FE + DET
FCS	0.0765	0.0579	0.1343	0.0753	0.1517	0.0562	0.1327
FM	0.0810	0.0480	0.1290	0.0621	0.1431	0.0522	0.1332
FP	0.0985	0.3096	0.4081	0.3981	0.4966	0.2108	0.3093
PCA	17.8045	0.0578	17.8623	0.0751	17.8796	0.0582	17.8627
ICA	24.3754	0.1089	24.4843	0.1372	24.5126	0.1877	24.5630
SPEC	0.0000	0.0705	0.0705	0.0943	0.0943	0.1020	0.1020
TOTAL		0.6527	43.0885	0.8422	43.2779	0.6671	43.1028

transform-based features (FCS, FP, FM) achieved the smallest time consumption compared with the other feature extraction methods. The time for the ICA and PCA feature extraction was longer than others. This method is not recommended for use in embedded systems or light computer systems because the algorithm is more complicated and time consuming. Among all of the Fourier transform-based feature extraction methods, FCS and FM consume less time compared with FP, because FCS and FM only utilize fast mathematical operations, such as addition, subtraction, and multiplication.

From the tables we can see that the MF detector consumes smaller time than other detectors when using the green nonwoven fabric. Table 2 summarizes the time consumption

regarding the feature extraction and target detection of the gray canvas tarps. As shown in Table 2, the FM feature extraction consumes the smallest time than other feature extraction methods. The time consumption found for MF and ACE detector was almost identical; however, the MF detector performed better than the ACE detector in terms of overall time consumption using all of the feature extraction methods. Table 3 shows the time consumption regarding the feature extraction and target detection of the white canvas tarps. As shown in Table 3, the FCS method displayed the smallest time consumption regarding the feature extraction. The time consumption for the ACE detector was higher compared with the GLRT and ACE detectors, whereas the difference between the ACE and MF speeds was small.

5 Conclusion and Future Works

This paper proposed feature extraction methods based on the Fourier transform called the FCS, FP, and FM. FCS is based on the coefficient selection, whereas FP is based on the phase, and FCS is based on the magnitude. Among all of these feature extraction methods, FCS showed the most consistent and high discrimination output of the ACE, GLRT, and MF target detectors. In terms of time consumption, the Fourier transform-based feature consumes significantly smaller time compared with standard feature extraction methods, such as PCA and ICA. For the target detectors, MF performance depended on the feature. MF only worked consistently with the original spectra or the vectors of the spectra. ACE and GLRT seemed to be unaffected by the spectra feature type and generated more stable and consistent results compared with MF. For future works, we would like to build our own target detector that can be optimized the Fourier domain-based feature.

References

1. D. Landgrebe, "Hyperspectral image data analysis," *IEEE Signal Process. Mag.* **19**(1), 17–28 (2002).
2. N. Renard, S. Bourennane, and J. Blanc-Talon, "Denoising and dimensionality reduction using multilinear tools for hyperspectral images," *IEEE Geosci. Rem. Sens. Lett.* **5**(2), 138–142 (2008).
3. M. O. Smith, P. E. Johnson, and J. B. Adams, "Quantitative determination of mineral types and abundances from reflectance spectra using principal components analysis," *J. Geophys. Res.* **90**, 797–804 (1985).
4. L. Molgedey and H. Schuster, "Separation of independent signals using time-delayed correlations," *Phys. Re. Lett.* **72**(23), 3634–3637 (1994).
5. F. Tsai and W. Philpot, "Derivative analysis of hyperspectral data," *Remote Sens. Environ.* **66**(1), 41–51 (1998).
6. L. M. Bruce, C. H. Koger, and J. Li, "Dimensionality reduction of hyperspectral data using discrete wavelet transform feature extraction," *IEEE Trans. Geosci. Rem. Sens.* **40**(10), 2331–2338 (2002).
7. V. Ojansivu and J. Heikkila, "Blur insensitive texture classification using local phase quantization," in *Proc. of 3rd ICISP'08*, Vol. 5099, pp. 236–243, Springer-Verlag, Berlin, Heidelberg (2008).
8. K.-M. Saipullah and D.-H. Kim, "A robust texture feature extraction using the localized angular phase," in *Multimedia Tools and Applications*, pp. 1–31, Springer, Netherlands (2011).
9. T. Kolenda, L. K. Hansen, and J. Larsen, "Signal detection using ICA: application to chat room topic spotting," in *Proc. Intl. Conf. on Independent Component Analysis and Blind Source Separation*, pp. 540–545 (2001).
10. K. M. Saipullah et al., "Texture classification by implementing blur, scale and grey shift insensitive texture descriptor based on local Fourier transform," in *Proc. of IWAIT 2010* p. 74, Kuala Lumpur, Malaysia (2010).
11. K. M Saipullah and D.-H. Kim, "Spectral dimensionality reduction based on intergrated bispectrum phase for hyperspectral image analysis," in *Proc. of the SPIE Remote Sensing*, Vol. 8180, 81801H, Czech Republic, Prague (2011).
12. F. Zhou, J.-J. Feng, and Q.-Y. Shi, "Texture feature based on local Fourier transform," in *Proc. of Intl. Conf. on Image Processing*, Vol.2, pp. 610–613 (2001).
13. K. Muzzammil et al., "Texture feature extractor based on 2D local Fourier transform," in *proc. 31th (Korea Information Processing Society) KIPS Spring Conf.*, Vol. 16, pp. 106–109, Pusan, Korea (2009).
14. D. Manolakis et al., "Is there a best hyperspectral detection algorithm?," *Proc. SPIE* **7334**, 733402 (2009).
15. E. J. Kelly, "An adaptive detection algorithm," *IEEE Trans. Aerosp. Electron. Syst.* **AES-22**(2), 115–127 (1986).
16. E. J. Kelly, "Adaptive detection in non-stationary interference, part III," *Technical Report 761*, MIT Lincoln Laboratory (1986).
17. S. Kraut and L. L. Scharf, "The CFAR adaptive subspace detector is a scale-invariant GLRT," *IEEE Trans. Signal Process.* **47**(9), 2538–2541 (1999).
18. S. Kraut, L. L. Scharf, and L. T. McWhorter, "Adaptive subspace detectors," *IEEE Trans. Signal Process.* **49**(1), 1–16 (2001).
19. D. Manolakis, D. Marden, and G. A. Shaw, "Hyperspectral image processing for automatic target detection applications," *Lincoln Laboratory J.* **14**(1), 76–116 (2003).
20. D. W. J. Stein et al., "Anomaly detection from hyperspectral imagery," *IEEE Signal Process. Mag.* **19**(1), 58–69 (2002).

Khairul Muzzammil Saipullah received his BS and MS degrees in electronics engineering from Inha University, South Korea. He is currently working as lecturer at University Teknikal Malaysia Melaka. His research interests are real-time image processing for embedded devices, remote sensing, medical image analysis, robot vision for autonomous aerial vehicle, and embedded systems.

Deok-Hwan Kim received his MS and PhD from Korea Advanced Institute of Science and Technology. He is a professor of Inha University in Korea. His research interest includes storage system, embedded systems, real-time image processing, medical image analysis, remote sensing, and brain computer interface.